A&A 412, 799–812 (2003)
DOI: 10.1051/0004-6361:20031484

Astronomy & Astrophysics

XMM-Newton light curves of the low-mass X-ray binary EXO 0748–676: Dips, eclipses, and bursts

J. Homan[1,3], R. Wijnands[2], and M. van den Berg[1,4]

[1] INAF/Osservatorio Astronomico di Brera, Via Bianchi 46, 23807 Merate (LC), Italy
[2] School of Physics and Astronomy, University of St Andrews, North Haugh, St Andrews Fife, KY16 9SS, Scotland, UK
e-mail: radw@st-andrews.ac.uk
[3] *Current address*: Center for Space Research, Massachusetts Institute of Technology, 77 Massachusetts Avenue, Cambridge, MA 02139, USA
[4] *Current address*: Harvard-Smithsonian Center for Astrophysics, 60 Garden Street, Cambridge, MA 02138, USA
e-mail: maureen@head.cfa.harvard.edu

Received 21 February 2003 / Accepted 2 September 2003

Abstract. We present an analysis of XMM–Newton light curves of the dipping, bursting, and eclipsing low-mass X-ray binary EXO 0748–676, focusing on the variability on time scales of seconds to hours. The observed variability can be roughly divided in three types: dips, eclipses and bursts. We find that the appearance of the latter two, depends strongly on the strength of the first. We show that the absorption dips change from spectrally hard to spectrally soft as they become deeper, which supports suggestions that the source is composed of a spectrally hard compact source and a spectrally soft extended source. The fast variability in the soft light curve indicates that the large structures causing the dips are made up of smaller absorption cores. We present the first clear detection with XMM–Newton of eclipses below 2 keV in this source, and show that dipping activity is apparently unrelated to the source luminosity. We also test several proposed models for the spectral evolution during dips and confirm the presence of a scatter/reflection component in the eclipse spectrum.

Key words. accretion, accretion discs – binaries: eclipsing – stars: individual: EXO 0748–676 – X-rays: stars

1. Introduction

Among the ∼150 known low-mass X-ray binaries (Liu et al. 2001), there are 11 whose light curves show irregular and sometimes periodic intensity dips. These dips usually are ascribed to obscuration of the central X-ray source by thickened regions in the outer disc, that result from the impact of the accretion flow from the companion star (White & Swank 1982; Walter et al. 1982). Four of the dip sources also show (partial) eclipses, which are due to obscuration of the central X-ray source and/or the accretion disc corona by the companion star. The observed dips and eclipses are related to the inclination at which those sources are seen, which is probably between 75° and 90° (Frank et al. 1987), depending on the exact properties of the two stars and the orbital parameters. Because of their inclination and the regular obscuration of the bright inner parts of the system, these sources provide a good opportunity to study the vertical and large scale structure of accretion flows in low-mass X-ray binaries.

The transient source EXO 0748–676 is currently the only active low-mass X-ray binary that shows both dips and eclipses. Although the source was discovered in 1985 during an EXOSAT slew (Parmar et al. 1985), it was detected in Einstein archival observations from May 1980 (Parmar et al. 1986); the source has probably remained active ever since, with 1–20 keV fluxes between $\sim 10^{-12}$ erg cm^{-2} s^{-1} (with Einstein; Parmar et al. 1986) and 1.5×10^{-9} erg cm^{-2} s^{-1} (peak of the 1985 outburst). Observations of type I X-ray bursts (Gottwald et al. 1986, 1987) demonstrate that the compact object is a neutron star. The eclipses and dips revealed an orbital period of 3.82 hr (Parmar et al. 1986). Depending on the stellar parameters, the eclipse duration (8.3 min) and the orbital period give a system inclination of 75–82°. With EXOSAT, dipping activity (up to 80% decrease in 2–10 keV intensity) was observed at orbital phases ∼0.8–0.2 and ∼0.65 (phase zero being the center of the eclipse), with shallower dips at other phases. ASCA observations revealed that at low energies (1–3 keV) dipping (up to 100%) is present around most of the orbital cycle (Church et al. 1998).

Observations with the Rossi X-ray Timing Explorer (RXTE) revealed the presence of quasi-periodic oscillations (QPOs) with frequencies of ∼0.4–3.0 Hz and 695 Hz (Homan et al. 1999; Homan & van der Klis 2000). The ∼1 Hz QPO was only observed at low luminosities; a similar type of QPO was

Send offprint requests to: J. Homan,
e-mail: jeroen@space.mit.edu

also seen in two other high-inclination systems (Jonker et al. 1999, 2000). This QPO is probably caused by an opaque structure on top of the accretion disc that orbits the central source at a distance of ∼1000 km, or by variations in the inner coronal flow as hydrodynamical simulations of the accretion disc corona show (Melia et al. 1991). The 695 Hz QPO, observed during a short period of increased luminosity early 1996, had properties similar to the kHz QPOs observed in many other neutron star sources (van der Klis 2000).

Using the Reflection Grating Spectrometer (RGS) on board XMM–Newton, Cottam et al. (2001) recently found emission and absorption features whose properties also suggest the presence of a thickened accretion disc with plasma orbiting high above the binary plane. In their 0.3–2.5 keV light curves no eclipses were seen at the expected times, which was confirmed by the apparent lack of eclipses in the 0.5–2 keV band of the XMM–Newton EPIC-MOS and EPIC-pn observations analyzed by Bonnet-Bidaud et al. (2001). Based on their results, the latter authors proposed a model in which the source is a superposition of a compact ($\sim 2 \times 10^8$ cm) spectrally hard Comptonizing corona and a more extended ($\sim 3 \times 10^{10}$ cm) spectrally soft thermal halo. Spectral variations are then caused by variations in the absorption that affects the hard spectral component more than the extended soft component. This is in contrast with previous models of the source consisting of a compact black body and extended Comptonized component (Church et al. 1998) or an absorbed plus un-absorbed Comptonized component (Parmar et al. 1986).

In this paper we present an analysis of XMM–Newton light curves, focusing on variations on time scales of seconds to hours, both at high (>2 keV) and low (<2 keV) energies.

2. Observations and analysis

For our analysis we used all XMM–Newton observations of EXO 0748–676 that were publicly available at the time of writing. Although XMM–Newton (Jansen et al. 2001) can observe simultaneously with different instruments, in many of our observations (all performed during the calibration and performance verification phase) data from one or more instruments are absent or incomplete. We decided to use either EPIC-MOS1 (Turner et al. 2001) or EPIC-pn (Strüder et al. 2001) data, depending on which of these cameras had the longest exposure. A log of the observations, including the instruments from which the data were used, is given in Table 1. Note that the instruments were used in a variety of modes and with different filters. An analysis of observations 1 and 2 has previously been published by Bonnet-Bidaud et al. (2001).

The MOS and PN data were reprocessed following the procedures described in the XMM–Newton data-analysis guides[1] and using the latest calibration data. Data were extracted from circles centered around the source, with radii of 90″ (MOS1) or 40″ (pn, in order to avoid the edges of the CCDs). Light curves were produced with a time resolution of 1 s and 10 s in the 0.3–10, 0.3–2 and 2–10 keV energy bands. The 10 s light curves are shown in Fig. 1. A colour was defined as the ratio of the count rates in the 2–10 keV and 0.3–10 keV bands, and colour curves were created by taking the running average of 30 s intervals. Background light curves were extracted in a similar fashion (same radius, same CCD), with the center of the extraction circle at a location were no source contribution is expected – background extraction from an annulus centered on the source, as is common practice, could not be performed, since the source was often located too close to the edge of the CCD. Variability in the background was never strong enough to warrant the exclusion of part of our data (see Fig. 1, gray lines). Note that the count rates shown in Figs. 1–4 are not background subtracted.

Table 1. Log of XMM–Newton observations and data of EXO 0748−676 used in this paper. From left to right: observation number for this paper, observation date with start and end time, the camera (EPIC-MOS1 or EPIC-pn) with mode and filter, and exposure time.

Obs.	Date and Start-End Time (TT)	Camera [Mode, Filter][a]	Exp. (ks)
1	2000-04-04 17:19–22:53	MOS1 [FF,T]	20.0
2	2000-04-21 03:59–09:04	PN [FF,M]	18.1
	2000-04-21 09:50–10:44	PN [LW,M]	3.2
	2000-04-21 15:22–20:24	PN [SW,M]	18.1
3	2001-02-03 17:32–19:32	MOS1 [FF,M]	7.2
	2001-02-04 01:23–11:54	MOS1 [FF,M]	21.6
4	2001-10-13 00:19–01:01[b]	MOS1 [FF,M]	32.9

[a] Mode: FF = Full Frame, LW = Large Window, SW = Small Window; Filter: T = Thick, M = Medium.
[b] Observation ended on 2001-10-14.

Due to the brightness of the source, significant pile-up occurred in our observations, especially in the last observation, where a clear hole could be seen in the center of the point spread function. To investigate the effects of the pile-up on the shape of light and colour curves, we made light curves by extracting data only from an annulus around the source position which excluded the piled-up core of the point spread function. We found that after scaling to the original count rates, within the statistics, those light and colour curves were indistinguishable from those made using the uncorrected data. In view of our statistics, we decided to use the initial light curves and not correct for pile-up. Because of the pile-up effects, which have a more serious effect on spectra than on light curves, we decided not to perform a detailed spectral analysis, except for the last exposure of obs. 2. Details of this analysis, which was performed with the aim of testing the spectral models of Church et al. (1998) and Bonnet-Bidaud et al. (2001), can be found in the appendix.

3. Results

In Fig. 1 we show the light curves of EXO 0748–676 in the 0.3–2 keV (soft) and 2–10 keV (hard) energy bands, together

[1] The XMM–Newton SOC *User's Guide of the XMM–Newton Science Analysis System* and *An Introduction to XMM–Newton Data Analysis* by the NASA/GSFC XMM–Newton GOF.

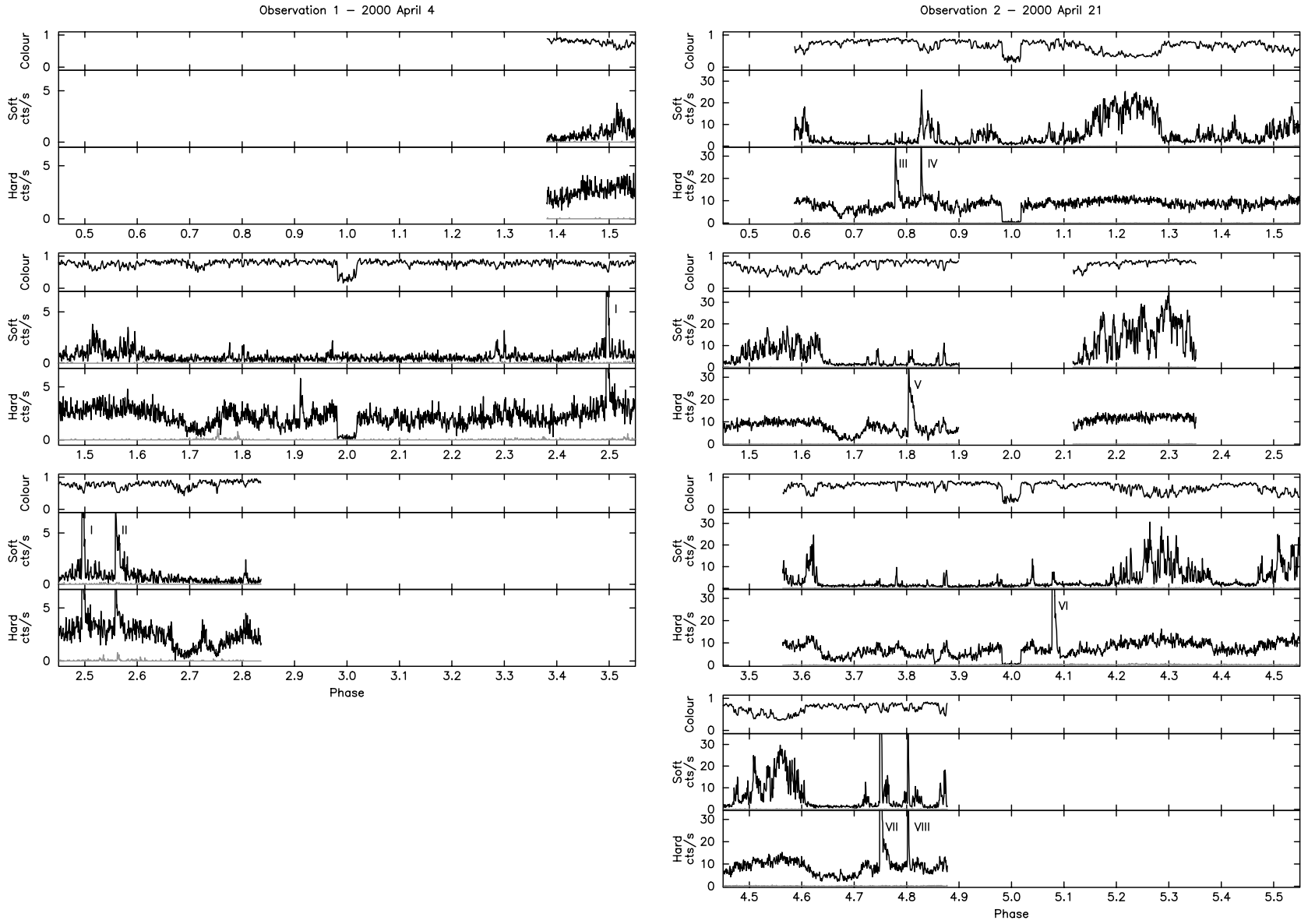

Fig. 1. XMM–Newton light and colour curves of EXO 0748-676 for the 2000 April 4 and 2000 April 21 observations. Each panel shows roughly one orbital cycle, with, from top to bottom, the colour curve, the 0.3–2 keV light curve, and the 2–10 keV light curve. For reference we also plot the background light curves (gray lines). The light curves have a time resolution of 10 s, whereas the colour curves show a 30 s running average. For clarity, error bars on the curves were omitted; they are in the order of $\sqrt{0.1 \times \text{count rate}}$. Type I X-ray bursts are indicated by Roman numerals.

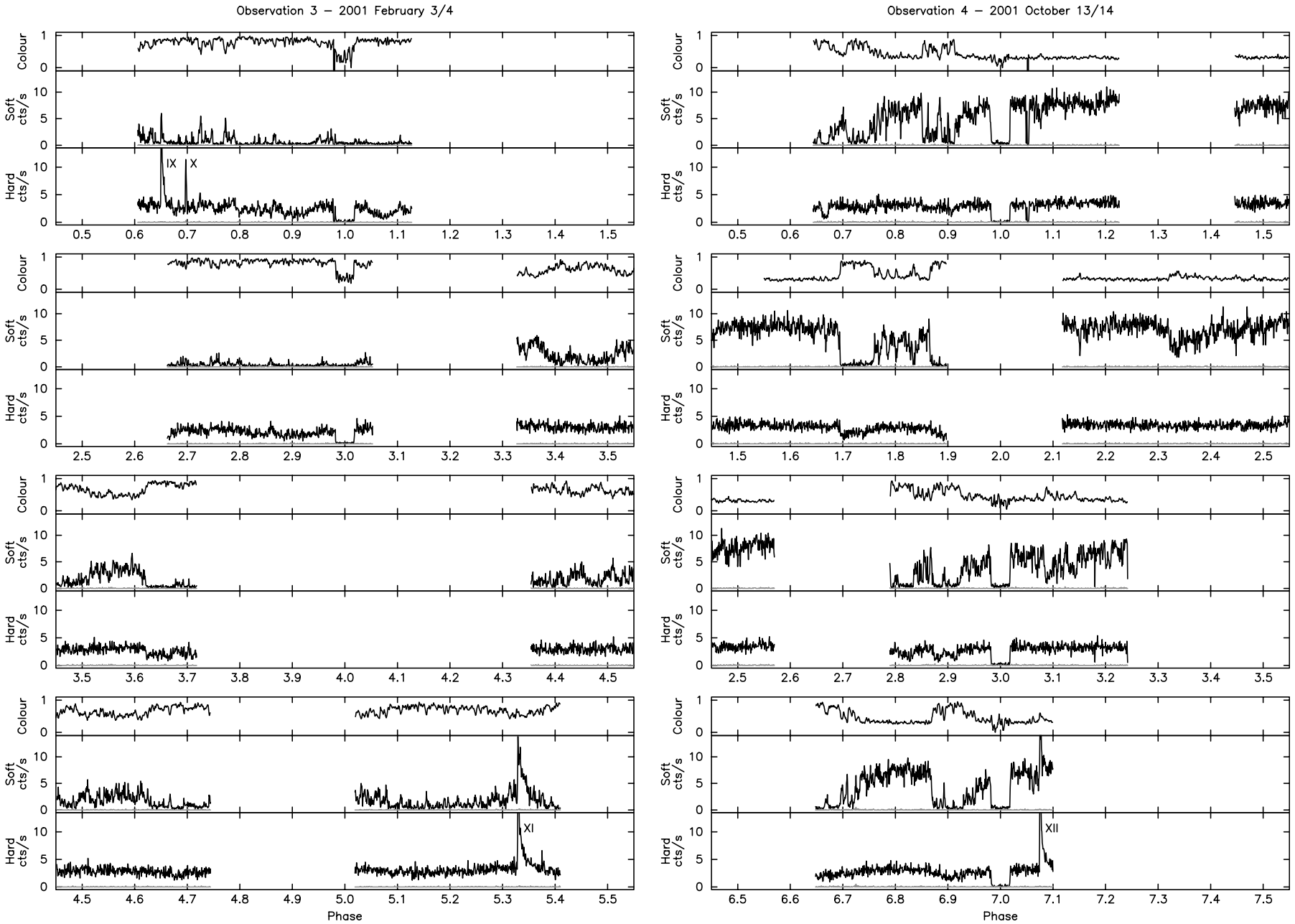

Fig. 1. (continued). Light and colour curves for the 2001 Feb. 3/4 and 2001 October 13/14 observations. The sharp dips in the first orbits of panels c (just before the eclipse ingress) and d (around phase 1.05), during which no counts were observed, are probably instrumental effects.

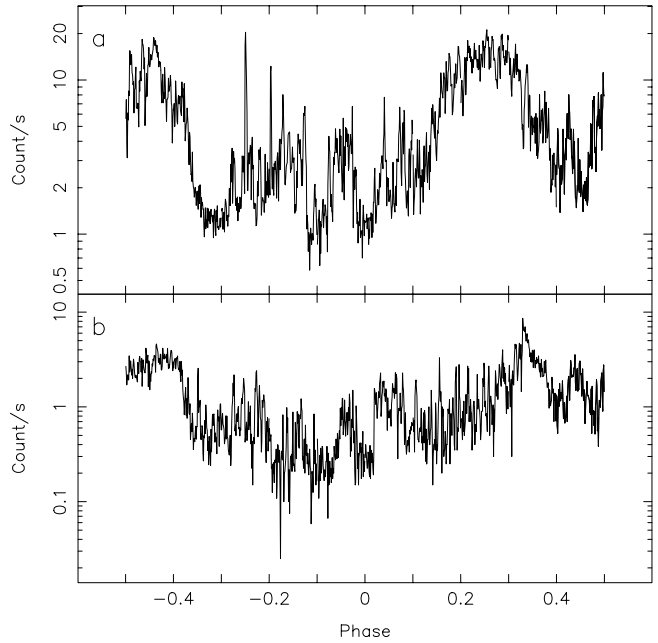

Fig. 2. Folded 0.3–2 keV light curves of observation 2 **a)** and observation 3 **b)**. The data were rebinned to 1000 bins per orbital cycle and, unlike Fig. 1, the count rate is plotted logarithmically. Type I bursts are still included. Weak eclipses are visible around phase zero.

with curves for the colour. Count rates are plotted versus orbital phase, with phase zero assigned to mid-eclipse. Note that, because of different instruments, filters, and CCDs, the count rates of the four observations should not be compared directly; observation 1 was done with a thick filter instead of a medium filter, and for observation 3 we used data from the EPIC-pn data, which is a more sensitive detector than the EPIC-MOS.

As was already noted by Bonnet-Bidaud et al. (2001), at first sight the soft and the hard light curves have little in common; the soft light curves show a lot of rapid activity, whereas the variations in the hard light curves, except for eclipses and type I X-ray bursts, are much slower and usually weaker.

3.1. Eclipses

While the RGS and EPIC data analyzed previously (Cottam et al. 2001; Bonnet-Bidaud et al. 2001) were characterized by the absence of eclipses at low (<2 keV) energies, our fourth observation (Fig. 1) is the first XMM–Newton light curve of EXO 0748–676 to show clear eclipses at low energies. In contrast to those in the soft band, the light curves in the hard band always show eclipses. It should be noted that in the folded light curves of observations 2 and 3 (shown in Fig. 2) during the phases of the eclipse the count rates in the soft band are actually below the average count rates for these observations (but not as low as some of the dips). Although not as apparent as in observation 4, this probably indicates that in these observations the effects of the eclipse *are* present. In both bands the eclipses are not total, with residual count rates of ∼5–8% and ∼4–5.5% in, respectively, the soft and hard band of the fourth observation. Typical ingress/egress times in observation 4 are ∼8–10 s (see Fig. 3), both in the soft and hard band. The folded 0.3–10 keV

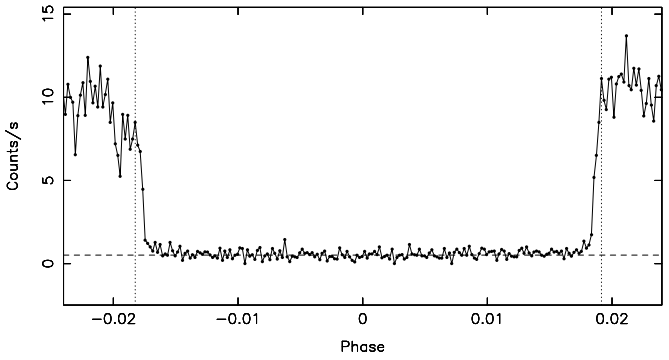

Fig. 3. An enlargement of part of the folded 0.3–10 keV light curve of observation 4. The time resolution is 2 s. The dashed line represent the average count rate from 200 data bins centered around phase zero. The dotted lines represent the start of eclipse ingress and the end of eclipse egress.

light curve of observation 4 (Fig. 3) also reveals the presence of structures at the end of the eclipse ingress and beginning if the eclipse egress, similar to the "shoulders" reported by Parmar et al. (1985).

3.2. Dips

Like in the ASCA observations analyzed by Church et al. (1998), dipping extends around most of the orbital phase and is most clearly visible in the soft band – only observation 4 shows several intervals in which the 0.3–2 keV light curve is dip-free. With dipping being present most of the time, the most eye-catching features in the soft band are periods during which the strength of the dipping is reduced. These decreases in the dipping are the soft flares reported by Cottam et al. (2001) and Bonnet-Bidaud et al. (2001). Periods of reduced dipping show two typical time scales; extended intervals, lasting typically for several minutes to an hour (Fig. 1) and shorter changes during those intervals, with time scales of seconds (Fig. 4a). When present, the extended intervals of (reduced) dipping in the soft and hard bands are probably related to the orbital phase; they appear at a relatively constant phase and are present for several consecutive orbits. This is most clearly seen in observation 2. Note that the interval of reduced dipping around phase 0.25 in this observation seems to show a slow, possibly random, shift towards higher phases; taking the moment during ingress at which the "saturation" level in the soft band is reached as a reference point, the ingress of the dipping interval at phases near 0.3, seems to occur at a later (∼3%) phase in subsequent orbits.

The phase extent and strength of the (decreases in) dipping undergo changes between orbital cycles. Unlike the long intervals, smaller structures do not seem to recur in later orbits – at least not at a similar phase. The rapid variations in the count rate in the soft band can be intense, with the count rate changing by factors of more than 10 on time scales of only a few seconds (see e.g. Fig. 4a) – they are most clearly observed in observations 2 and 4. Excluding type I X-ray bursts and eclipses, the dynamical range (defined as the maximum count rate divided by minimum count rate, within one observation)

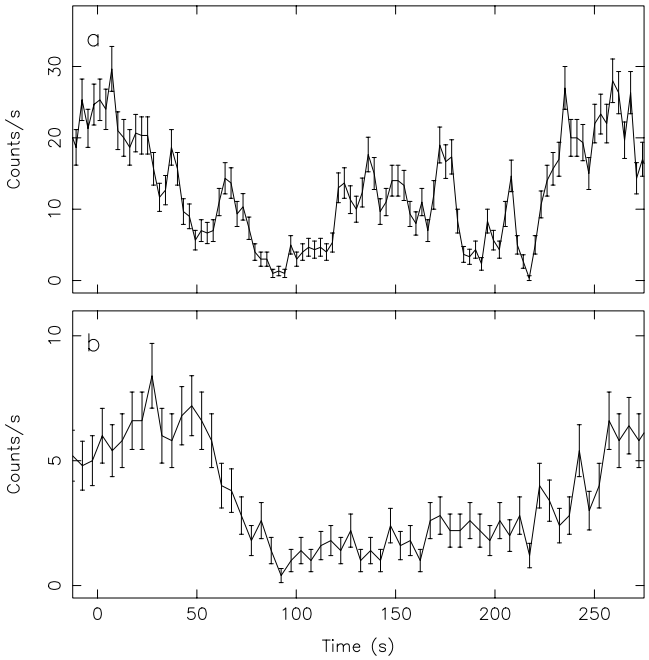

Fig. 4. Light curves showing the fastest observed dipping events in the 0.3–2 keV **a)** and 2–10 keV **b)** bands. The 0.3−2 keV data are taken from observation 2 around phase 2.2 and have a time resolution of 3 s; the 2–10 keV are taken from the same observation around phase 3.85 and have a time resolution of 5 s.

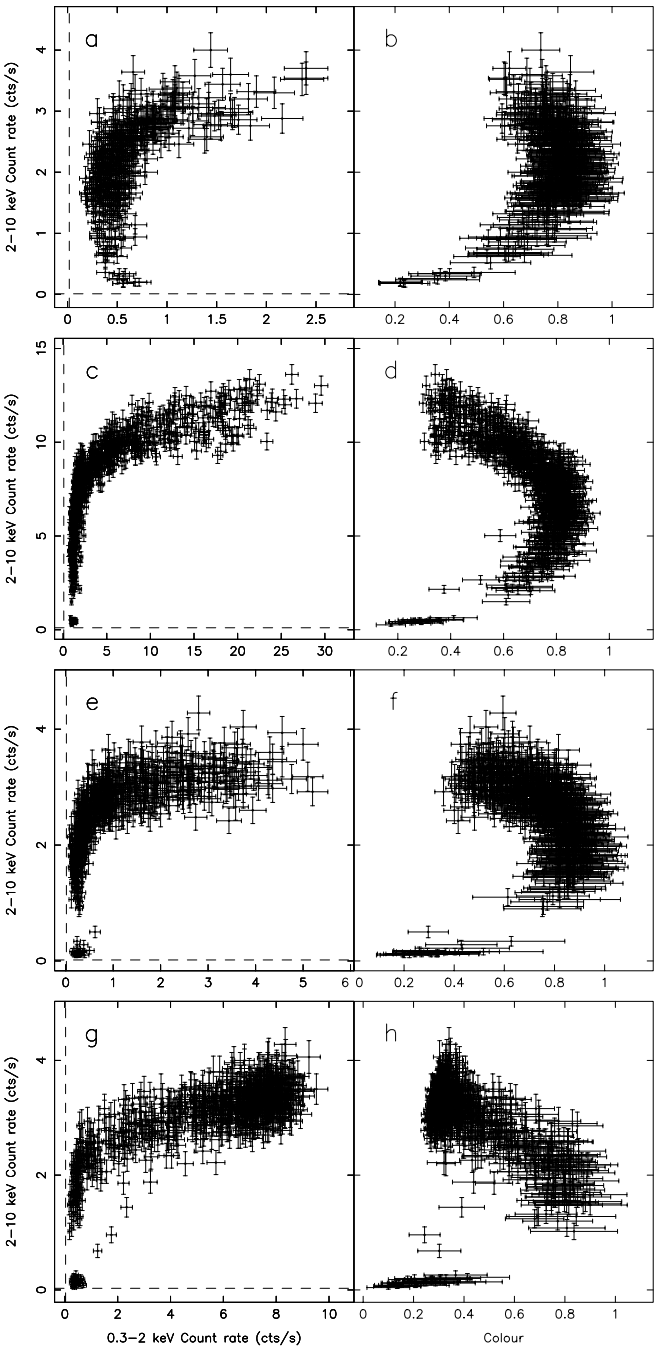

Fig. 5. Left panels: 2–10 keV count rate vs. 0.3–2 keV count rate, right panels: 2–10 keV count rate vs. colour. From top to bottom: observations 1, 2, 3, and 4. Each point represents a 50 s average. The two dashed lines in the left panels represent the average background count rates in the two energy bands. The eclipses can be seen as small detached blobs. Note that while the count rates in the soft band during the eclipse are similar to those during the dips, they are clearly lower for the hard band.

of the soft band is >110. Variations in the hard band, seem to be more modest; the dynamical range is only ∼30, and strong/violent short-time variations, like those seen in the soft band, are not observed. For comparison we show the fastest observed dips in the soft and hard bands in Fig. 4; with a dip ingress of more than 30 s the fastest dip in the hard band is considerably slower than those in the soft band, which can be as fast as a few seconds. During the low count rate periods (including the eclipses) the source is detected well above the background in the 0.3–2 keV band, with minima (observations 3 and 4) of ∼0.1–0.3 cts s^{-1}, compared to background count rates of ∼0.01–0.03 cts s^{-1}.

As expected, the hard band is less affected by the dipping than the soft band. Dips in the hard band are only (but not always) observed when the count rate in the soft band is at a minimum. They are mostly observed at the phases around 0.7 and 0.9, which are also the phases which show the least variability and the lowest count rates in the soft band. The relation between dipping in the soft and hard band is clarified when we plot the count rates in the hard and soft band against each other, as has been done in Fig. 5; high count rates in the soft band are only found when the count rate in the hard band is high (i.e. outside dips). Dips in the soft count rate are however not always visible as dips in the hard band. During dips in the hard band the count rate does not drop below the level found in eclipses, whereas in the soft band the source can occasionally be weaker than during eclipse (see also Fig. 2). In all four observations the spectrum initially hardens as the count rate decreases, until the hard band starts to be affected, after which the spectrum starts to soften (see also Fig. A.2). It is also interesting to see that in observation 4 the colour saturates at the highest count rates and that the spectrum during the eclipse is softer than this saturation level. The motion of the source along the tracks in Fig. 5 is smooth, in the sense that (except during eclipses) the source never jumps from one end of the track to the other.

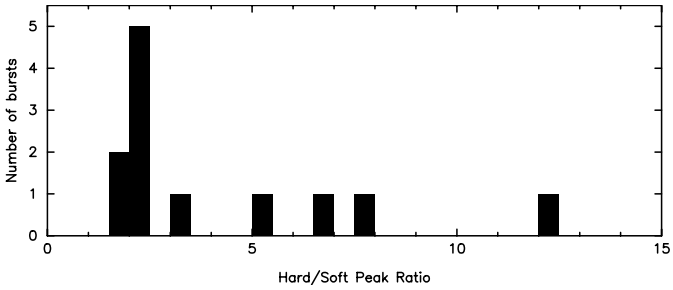

Fig. 6. Histogram showing the observed ratio of peak count rates of the hard and soft bands for the 12 observed type I X-ray bursts. See also Table 2.

Table 2. Peak count rates of the 12 observed type I X-ray bursts in the soft (0.3–2 keV) and hard (2–10 keV) X-ray bands, together with their hard/soft ratio. Indicated is whether the bursts occurred during intervals of reduced dipping or full dipping (corresponding to the lowest count rates in the soft band, and, as opposed to reduced dips, sometimes also visible as dips in the hard band). For bursts I, II, and VII this was not completely clear. See Fig. 1 for the labeling (I–XII) of the bursts.

Burst	Pers.[a]	Soft peak	Hard peak	Ratio
I	R(?)	9.8 ± 1.4	19.8 ± 2.0	2.0 ± 0.4
II	R(?)	8.8 ± 1.3	18.4 ± 1.9	2.1 ± 0.4
III	F	8.4 ± 1.3	42.0 ± 2.9	5.0 ± 0.8
IV	R	20.6 ± 2.0	43.0 ± 2.9	2.1 ± 0.3
V	F	5.0 ± 1.0	38.0 ± 2.8	7.6 ± 1.6
VI	F	8.6 ± 1.3	104 ± 5	12.1 ± 1.9
VII	R(?)	87.4 ± 4.2	162 ± 6	1.9 ± 0.1
VIII	R	56.0 ± 3.3	99.4 ± 4.5	1.8 ± 0.1
IX	F	8.0 ± 1.3	27.0 ± 2.3	3.4 ± 0.6
X	F	1.8 ± 0.6	12.4 ± 1.6	6.9 ± 2.5
XI	R	10.8 ± 0.5	24.4 ± 2.2	2.3 ± 0.2
XII	R	15.0 ± 1.7	30.4 ± 2.5	2.0 ± 0.3

[a] Type of persistent emission in the soft band during which the burst occurred; R = Reduced dipping, F = Full dipping.

3.3. Type I X-ray bursts

In total 12 type I X-ray bursts were observed, 8 of which occurred in pairs with a separation of ∼10.65–14.65 min. When comparing the X-ray bursts in the hard and soft band we find that some of them hardly show up in the soft band. To illustrate this, we give the ratios of the hard peak and soft peak count rates for all 12 bursts in Table 2 and plot them in Fig. 6. Count rates were obtained from 5 s running averages to reduce the scatter in the 1 s light curves. As no correlation was found between total count rate and the ratio of the peak count rates in the two bands, we assume that the effects of pile-up on our results are negligible. The peaks in the hard and soft band did not occur simultaneously – the quoted count rates are those at the time of the hard peak. Taking the soft count rates from the peak in the soft band (which occurred between 9 s before and 7 s after that in the hard band) results in a similar picture. A clear concentration (7 out of 12) of bursts is present around a hard/soft peak ratio of ∼2, with the other bursts all having larger values. While due to the rapid nature of the dips, it is not possible to rule out that some of the burst occurred during short periods of reduced dipping (which have similar time scales as the bursts), it seems that the 5 bursts that have ratios larger than 3 all occur during dipping intervals. Note that the small peak around phase 1.9 in the hard band of observation 1 was not included, since the nature of this peak was not clear. If this peak, which occurred during a dip in the hard band, also was a type I burst its hard/soft ratio would be even higher than that for burst VI.

3.4. Fluxes

In order to compare the fluxes of the four observations as well as possible, we fitted the spectra of the source during the parts of the observations with the highest count rates. The spectra were fitted in XSPEC with various models. While most models provided good fits in the 5–10 keV range, we were not able to satisfactorily fit the low energy parts of the spectrum with a consistent model (see also Appendix). For all four observations the unabsorbed 5–10 keV flux was consistent with 9×10^{-11} erg cm^{-2} s^{-1}. Our fits suggest that differences at lower energies are likely due to the complex effects of absorption.

4. Discussion

While at first sight the count-rate variations at low and high energies in EXO 0748–676 seem to occur independently from each other (Fig. 1), they are in fact strongly related (Fig. 2) and likely due to the same mechanism. This is supported by the fact that the source moves smoothly along the tracks in Fig. 2, which suggests that most of the variations in the light curve are caused by changes in only one parameter. In this section we discuss how changes in the absorption can account for the observed variations as well as for the appearance of the eclipses and type I X-ray bursts.

4.1. Dips, eclipses, and bursts

Both Church et al. (1998) (ASCA observations) and Bonnet-Bidaud et al. (2001) (XMM–Newton observations) showed that the spectral evolution of EXO 0748–676 can be largely explained by the effects of variable absorption progressively covering two (stable) emission components. In both models the extended component is spectrally softer than the compact central source and as such both are consistent with the observed behavior. However, as we show in the Appendix, the real spectral composition is likely to be more complex than suggested by Church et al. (1998) or Bonnet-Bidaud et al. (2001).

As absorption is intrinsically less efficient at high energies, dipping is most pronounced at low energies and therefore spectrally hard. This can clearly be seen in our observations 1–3 and in the ASCA light curves of Church et al. (1998), in which dipping in the low energy bands extends over a much larger phase than in the high energy bands; the intervals of rapid increases in the count rate in observations 1–3 and most of observation 4

represent periods in which the absorption is reduced by a significant fraction. One would expect the ingress of dips in the soft band to precede that in the hard band, an effect that is indeed seen in our light curves and even more clearly demonstrated in Fig. 5. We therefore prefer to refer to the intervals of increased count rate as periods of reduced dipping instead of flaring, since we think this gives a better description of what gives rise to the changes in the light curves.

Bonnet-Bidaud et al. (2001) suggested that part of the variability in their "flares" is due to intrinsic changes in the halo luminosity (possibly due to reprocessing of type I X-ray bursts). However, the fact that the count rates in the eclipse in observation 4 are similar to those in observation 3, which had the same instrumental setup but was much less luminous outside the dips in the soft band, suggests (assuming that the same part of the halo was left uncovered during the eclipse) that the halo luminosity did in fact not vary significantly. Moreover, since the "flares" occur at similar phases for several orbits, delayed reprocessing of type I X-ray bursts is basically ruled out as a trigger for halo-luminosity changes.

The apparent lack of eclipses in the soft band of the first three observations can easily be explained; the additional absorption column presented by the companion star has almost no influence below 2 keV, since most of the soft flux from the central source was already absorbed at the time of eclipse – the projected size of the halo also has to be significantly larger than that of the companion star to not be affected during an eclipse. The fact that the count rates outside of the eclipse are sometimes lower than those during the eclipse suggests that the absorbing structures, as seen from the central source, occasionally subtend a larger solid angle than the companion star. This indicates that in the vertical direction the absorbing material extends well beyond the expected scale height of a thin disc.

The behavior of the type I X-ray bursts can also be explained in this framework; when they occur during intense dipping intervals, i.e. when absorption is high, the soft flux of the burst is more affected than the hard flux, resulting in ratios larger than 2. Those that occur during intervals of reduced dipping are affected less by absorption, resulting in ratios of ∼2, which is apparently the normal ratio for these bursts in this source. The spread in ratios larger than 2 probably reflects various stages of absorption. We note that many of the bursts analyzed by (Cottam et al. 2002), which showed red-shifted absorption lines, occurred during periods of significant absorption below 2 keV.

4.2. Location of the absorbing material

Since we know that the absorbing material has a height of more than 8–15° above the orbital plane it has to be constantly refreshed in order to be visible at a more or less fixed position in the orbital frame, for at least several orbital cycles; if not, it would disappear on a time scale that is shorter than the orbital period, because the time scale for changes in the vertical scale height in the accretion disc is comparable to the dynamical time scale (Frank et al. 1992). Building on the work of Lubow & Shu (1976), Frank et al. (1987) proposed a model in which an accretion stream overshooting the point of impact with the disc settles in a ring-like structure at a radius of $\sim 10^{10}$ cm (for a 1.4 $M_\odot$ neutron star and $P_{\rm orb}$ = 3.82 hr). As the result of an ionization instability, a two-phase medium is formed, which consists of a hot thin gas and cool clouds and is present between phases 0.3 (at which the material joins the disc) and 0.8. The presence of such a two-phase absorber, consisting of both neutral and ionized gas, seems to be confirmed by recent Chandra observations of the source (Jimenez-Garate et al. 2003). If we apply the equations of Frank et al. (1987) to EXO 0748-676, we find a typical size for the cool clouds of 4×10^7 cm and a column density of 6×10^{23} cm^{-2}. At a distance of 10^{10} cm this should cause dips with a time scale of ∼1 s, quite similar to the shortest observed time scales. While these clouds can explain the rapid variations in the soft band, they cannot (within this model) explain the occurrence of dipping at phases between 0.8 and 0.3.

Another possible site of absorbing structures could be a thickened disc rim; Retter et al. (2002) found that the dips in the high-inclination X-ray binary X1916–053 are responsible for the positive superhump period observed in the X-rays and optical. They suggest that a thickened disc rim can explain both the X-ray and optical superhump. Positive superhumps (quasi-periodicities a few percent longer than the orbital period) are observed in some cataclysmic variables (Warner 1995) and low-mass X-ray binaries (O'Donoghue & Charles 1996) and are interpreted as a signature of an eccentric precessing accretion disc. Evidence for such superhumps may be present in observation 2 in the form of dipping intervals shifting in phase (see Sect. 3.2). However, the phase shift of these dips might as well be a random effect; unfortunately, the data sets for the other observations either are too short or contain too many gaps to study this in more detail.

Whatever the exact nature of the absorbing material is, the fourth observation shows that its structure and/or presence can change considerably on time scales shorter than eight months (which is the interval between observations 3 and 4). It is not clear what causes these changes. The 5–10 keV fluxes during the brightest intervals of each observation are consistent with each other, suggesting that, if proportional to the 5–10 keV flux, the mass accretion rate remained constant. A possible explanation could be the precession of a tilted accretion disc, evidence for which has been found in several other low-mass X-ray binaries (e.g. Larwood 1998, and references therein). A tilted accretion disk, and hence precession, may also be present in EXO 0748−676 as was suggested by Crampton et al. (1986) on the basis of optical observations. If true, the absorbing structures could remain unchanged, but depending on the phase of the precession more (or less) of the absorbing material moves through our line of sight.

4.3. Constraints from time scales

The ingress and egress time scales we observed during the eclipses are on the order of ∼8−10 s, somewhat larger but consistent with values obtained with EXOSAT and RXTE (Parmar et al. 1986; Hertz et al. 1997). Depending on the density profile of the companion star's outer atmosphere (see a discussion on this topic in Parmar et al. 1986), this means that

92–95% of the 0.3–10 keV flux and 94.5–96% of the 2–10 keV flux originates in a region with a radius of $3.5–3.9 \times 10^8$ cm or smaller. The latter number is obtained from the duration of the eclipse ingress and egress; depending on the properties of the secondary (see Parmar et al. 1986), binary parameters (such as secondary's radius, binary separation and inclination) were derived, which, using the eclipse time scales, translated into upper limits on the size of the eclipsed central object. As was already found by Parmar et al. (1986), near the bottom level of the eclipse, the eclipse ingress and egress progress slower than at the higher count rate levels (Fig. 3). This cannot be due to the density profile of the secondary's atmosphere, and suggests a central source geometry that is at least partly extended.

The shortest time scales in the soft band are on the order of a few seconds and those in the hard band are ∼30 s. These time scales are difficult to interpret, since the distance from the central source and velocity across our line of sight of the absorbing material are not well known. However, the time scales for the dips in the soft band, which are shorter than the eclipse ingress and egress times, suggest that the central region is smaller than the values given above. The shortest observed time scales for the two bands are quite different. This difference can be explained if we assume that the absorbing material consists of small clouds (patchy absorber) as in the model of Frank et al. (1987) discussed above, each with a density high enough to considerably affect the soft flux, but not the hard flux. As the absorbing material (containing the small clouds) starts moving into our line of sight, the soft band is immediately affected, but it takes more time to have the required number of clouds present in our line of sight to affect the hard flux. An additional effect of such a patchy absorber is that the variations in the soft band are much stronger than in the hard band – quite the opposite of what is found for other types of variability in X-ray binaries, which usually get stronger towards higher energies.

4.4. Residual emission

From Figs. 1 and 5 it is clear that eclipses and dips in the soft and hard band both tend to saturate at a level that is significantly above the background. Part of this residual flux can be attributed to (fluorescent) emission from the extended thermal halo (Cottam et al. 2001; Bonnet-Bidaud et al. 2001). However, as suggested by observations of type I X-ray bursts during eclipses in EXO 0748–676 (Parmar et al. 1985; Gottwald et al. 1987), ∼4% of the 2–6 keV flux from the central source is scattered into our line of sight during eclipse. This scattering occurs in the accretion disc corona, which might be the same component as the extended thermal halo, and accounts for most of the residual flux in the hard band; residual emission in the hard band during eclipses in observation 4 is also ∼4%. The slightly higher fraction of residual flux in the soft band (compared to the hard band) can be attributed to additional emission from the extended thermal plasma present above the disc.

5. Summary

We have analyzed XMM-Newton light curves of the low-mass X-ray binary EXO 0748-676. We find that the appearance of the light curves in the soft and hard band can be well explained by progressive absorption of two spectral components. From the colour of the residual emission during eclipses, and from the colour evolution with increasing degree of absorption, we conclude that the source contains an extended source of X-ray emission that is spectrally softer than the compact source, as suggested earlier by Church et al. (1998) and Bonnet-Bidaud et al. (2001).

In the soft band, the count rate during dipping intervals sometimes decreases below the level during eclipses, while the source is always detected well above the background, both in the soft and hard band. This implies that (at certain phases) the absorbing material as seen from the central source, subtends a larger solid angle than the projection of the companion star, but that it is smaller than the extended soft component. The recurrence of dipping structures in the light curves in consecutive orbits indicates that the absorbing material can maintain a more or less fixed position in the corotating frame for at least several orbits. However, the drastic change of appearance in the light curve of October 2001 with respect to that of February 2001, indicates that the position and/or density of the absorbing material can vary within months. The difference in the shortest time scales for dipping activity in the soft and hard band, suggests that the dipping is caused by a patchy absorber that affects soft energies more efficiently.

Future observations with XMM–Newton, in particular for several continuous orbital periods, may shed more light on the possible presence of superhumps and on the evolution and structure of the absorbing material.

Acknowledgements. JH acknowledges support from Cofin grants 2001/MM02C71842 and 2001/028773. MvdB acknowledges financial support from the Italian Space Agency and MIUR. This work is based on observations obtained with XMM-Newton, an ESA science mission with instruments and contributions directly funded by ESA member states and the USA (NASA).

Appendix A: Spectral analysis

Several attempts have been made in the past to model the spectral evolution of EXO 0748–676 as a function of increasing absorption. In this appendix we test the models by Church et al. (1998) and Bonnet-Bidaud et al. (2001) that were already discussed extensively in the main text. Although the soft-band light curves presented earlier in this paper and the recent spectral results by Jimenez-Garate et al. (2003) strongly suggests that the obscuring medium is far from being uniform, these models treat the absorber as having a smooth density profile. Moreover, the extended components that are part of the two models are assumed to have a uniform brightness. Notwithstanding these simplifications we feel that a vigorous test of the two models may yield important information on the structure of the central source and the absorber.

A.1. Data reduction

For our spectral analysis we used the small-window mode EPIC-pn data of obs. 2 (i.e. the third data segment), the only

Table A.1. Time and count rate selections used for our spectral analysis. These selections are also displayed in Fig. A.1. Note that the eclipse (E) is excluded from the L1 count rate selection.

Selection	Time[a] (TT)	0.3–10 keV count rate (cts/s)
E	16:58:40–17:05:20	—
F1	17:42:30–18:30:00	—
Q	18:30:00–18:48:40	—
F2	18:48:40–19:23:40	—
D	19:23:40–19:45:20	—
L1	—	1.0–6.0
L2	—	6.0–12.5
L3	—	12.5–17.5
L4	—	22.5–27.5
L5	—	25.0–45.0

[a] Time on April 21 2000.

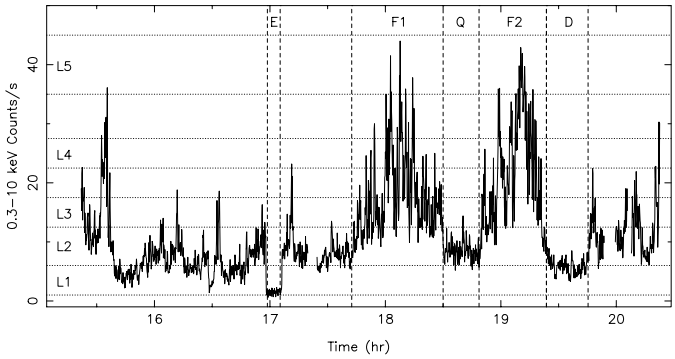

Fig. A.1. Light curve of the third data segment of obs. 2 (0.3–10 keV) showing the time and count-rate selections applied for our spectral analysis. Type I X-ray bursts are not shown. The labels L1-L5 indicate the count rate level selections (see main text). The other labels indicate the time selections and stand for eclipse (E), flaring interval 1 (F1), quiescence (Q), flaring interval 2 (F2), and dip (D). Note that the eclipse was not included in the L1 count rate selection.

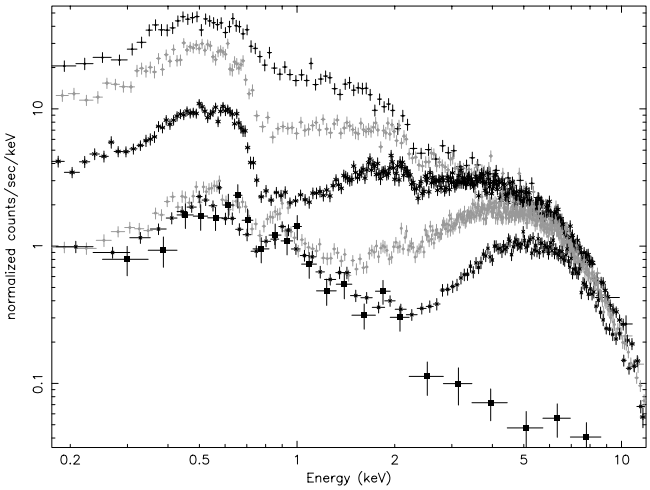

Fig. A.2. Energy spectra for the 5 count rate selections and the eclipse interval. From top to bottom: the spectra for the selections L5 to L1, and the eclipse spectrum (big filled square symbols). All spectra are rebinned for display purposes.

part of our data set that was not affected by pile-up. Source data were extracted from a circle with a 38″ radius, centered around the source; background data from a similar circle in the opposite corner of the window. Only events with pattern 0–4 were selected and data from bursts were discarded. Data were selected either on time or the 0.3–10 keV count rate; the times and count rates for the various selections can be found and seen in Table A.1 and Fig. A.1. Note that our time selections include those made by Bonnet-Bidaud et al. (2001) (F1, Q, F2, D) with the addition of an eclipse spectrum (E). The count rate selections, which do not cover the entire count rate range (see gaps in Fig. A.1) were converted to time intervals using a 10 s 0.3–10 keV light curve. The resulting spectra were fitted with the xspec package (Arnaud 1996,V11.2) with the models described below, using a canned response matrix. The ancillary response file was created using `arfgen`.

Before we discuss our spectral fits, some comments should be made on the two selection methods. First, selecting spectra based on temporal behavior (e.g. dipping activity), as was done by Bonnet-Bidaud et al. (2001) (see selections F1 and F2), will result in mixing of spectra with rather different properties; as is clearly illustrated by Fig. 5, spectral proprieties can change considerably with count rate. Selecting (narrow) count rate intervals, as was done by Church et al. (1998), will reduce these problems a bit, but mixing still occurs in those intervals where the count rate does not correlate with colour. Second, from other low-mass X-ray binaries we know that spectral evolution of the central source can occur on time scales that are considerably shorter than the exposure we analyzed (i.e. a few hours). Spectra that were taken more than a few hours apart, and which therefore have likely different central source properties, could end up having similar count rates because of the varying absorption, resulting in the mixing of different spectral properties. Unfortunately, tracing changes in the central source spectrum would require splitting our exposure in shorter pieces, resulting in a low statistical quality of the spectra.

A.2. Spectral fits

The eclipse spectrum and the count-rate selected spectra are shown in Fig. A.2. For a display of the time selected spectra we refer to Fig. 4 of Bonnet-Bidaud et al. (2001). Figure A.2 clearly shows that, when going to lower count rate selections (from L5 to L3) the spectrum above ∼3 keV remains largely unchanged, explaining the hardening of the spectrum (see Fig. 5). From L3 to L1 that part of the spectrum also starts to become affected, which, because of the saturation at low energies (compare L2 and L1 spectra), leads to a softening of the spectrum. The eclipse spectrum nicely shows that the soft part of the spectrum is consistent with that of the deepest dips, whereas at high energies the source is almost completely obscured (compare eclipse and L1 spectra).

Spectral fits were made with the models used by Church et al. (1998) and Bonnet-Bidaud et al. (2001). The first model

Table A.2. Spectral fit results. Models and energy ranges are given for each of the fits. Lower limits on ABB are 90% confidence. All other errors represent 1σ confidence intervals.

	Model: Church et al. (1998) Range: 0.8–10 keV $\chi^2_{\rm red}$/d.o.f. = 1.01/1594			Model: Church et al. (1998) + Gaussian Range: 0.15–12 keV $\chi^2_{\rm red}$/d.o.f. = 1.18/1916		
	L5	L3	L1	L5	L3	L1
ABB ([a])	0.01(19)	0.2(2)	>32	0.01(2)	4.2(4)	>91
$kT_{\rm bb}$ (keV)	1.6(1)			1.46(4)		
$N_{\rm bb}$ ([b])	$6.5(4)\times10^{-5}$			$6.8(2)\times10^{-5}$		
AGA ([a])	0.010(4)			0.031(2)		
APL ([a])	0.4(4)	3.2(1)	14.0(4)	0.12(1)	2.43(5)	13.7(2)
f	$0.09^{+0.46}_{-0.07}$	0.90(2)	0.955(2)	0.4(3)	0.853(1)	0.963(1)
$\Gamma_{\rm pl}$	1.33(1)			1.31(1)		
$N_{\rm pl}$ ([c])	0.0181(4)			0.0177(1)		
$E_{\rm line}$ (keV)	–	–	–	0.524(2)		
$\sigma_{\rm line}$ (keV)	–	–	–	0.103(2)		
$N_{\rm line}$ ([d])	–	–	–	0.032(1)		

[a] 10^{22} atoms cm^{-2}; [b] $L_{39}/(D_{10})^2$, with L_{39} the luminosity (10^{39} ergs s^{-1}) and D_{10} the source distance (10 kpc); [c] photons keV^{-1} cm^{-2} s^{-1} at 1 keV; [d] total photons cm^{-2} s^{-1} in the line.

was only used in conjunction with the count-rate selected spectra (L1–L5), whereas the Bonnet-Bidaud et al. (2001) model was used for both types of selection (to study the effect of selection method).

A.2.1. Church et al. (1998) model

The Church et al. (1998) model consists of a black body component from the neutron star, plus Comptonized emission from an extended and progressively covered accretion disc corona (ADC): ABB*BB + APL*f*PL + AGA*(1-f)*PL, where BB and PL are the black body and power-law terms, AGA the Galactic absorption term, ABB and APL the variable black body and power-law absorption terms, and f the progressive covering fraction of the ADC. Note that in this definition of the model ABB and APL include Galactic absorption and that the two PL components represent the covered and uncovered parts of the same spectral component. In all fits with this model the columns densities (ABB, AGA and APL) have a lower limit of 10^{20} atoms cm^{-2}, which is a factor of ∼10 lower than the average galactic column density in the direction of EXO 0748−676 (Dickey & Lockman 1990). AGA and the parameters for the black body and the power law were treated as single parameters for all spectra.

We started by performing fits to the L1, L3 and L5 spectra in the energy range used by Church et al. (1998) (0.8−10 keV). Figure A.3a shows the results of this fit; the best-fit parameters can be found in Table A.2. The $\chi^2_{\rm red}$/d.o.f. of 1.01/1594 is good, although ABB for spectrum L3 seems to be too low, given the covering fraction of 90% that we find. More worrisome are the unacceptably large residuals below 1 keV and also around 1.6 keV in the fit to spectrum L1. This part of the spectrum is not shown in Fig. 3 of Church et al. (1998), so we cannot check whether such residuals were also present in their fits to the ASCA data. Most likely, these residuals are due to the soft excess found by Thomas et al. (1997) and also discussed by Church et al. (1998). The presence of the this soft component is much clearer in the 0.15–12 keV spectra and a fit with the model in this energy range is clearly worse than in the 0.8−10 keV band ($\chi^2_{\rm red}$ = 1.76). Following Church et al. (1998) we add a Gaussian line to the model, which, like the power law component, is progressively covered. The best fit with this model is shown in Fig. A.3b; the best-fit parameters can be found in Table A.2. Again, even though the $\chi^2_{\rm red}$ = 1.18 is acceptable, large (localized) residuals are present − this time in the fits to all three spectra. As a general remark we note, that since most data bins are in the rather featureless part of the spectrum above a few keV, which is fitted well by the models, the residuals below 2 keV (which is the part of the spectrum we are most interested in) have only a limited effect on the $\chi^2_{\rm red}$.

When plotting the separate spectral components it becomes clear that rather than being a narrow line, the Gaussian is very broad and fits a large part of the continuum below 1 keV. Moreover, the ADC component dominates the spectrum over the entire energy range in all three spectra. The covering fraction and the two separate absorption components (AGA and APL) act in such a way on the ADC component that the uncovered power law (together with the Gaussian) fits the low energy part of the spectrum, whereas the covered power law fits the high energy part. In the L5 spectrum the black body component only contributes 20% of the absorbed 0.15−12 keV flux.

A.2.2. Bonnet-Bidaud et al. (2001) model

In the Bonnet-Bidaud et al. (2001) model the source consists of a spectrally hard compact central component and a spectrally soft extended component. These are modeled, respectively, by a power law (PL) and a thermal Raymond-Smith model (RS), each affected by their own absorption component: APL*PL + ARS*RS, where APL and ARS both include the galactic absorption and are not allowed to become lower than 10^{20} atoms cm^{-2}.

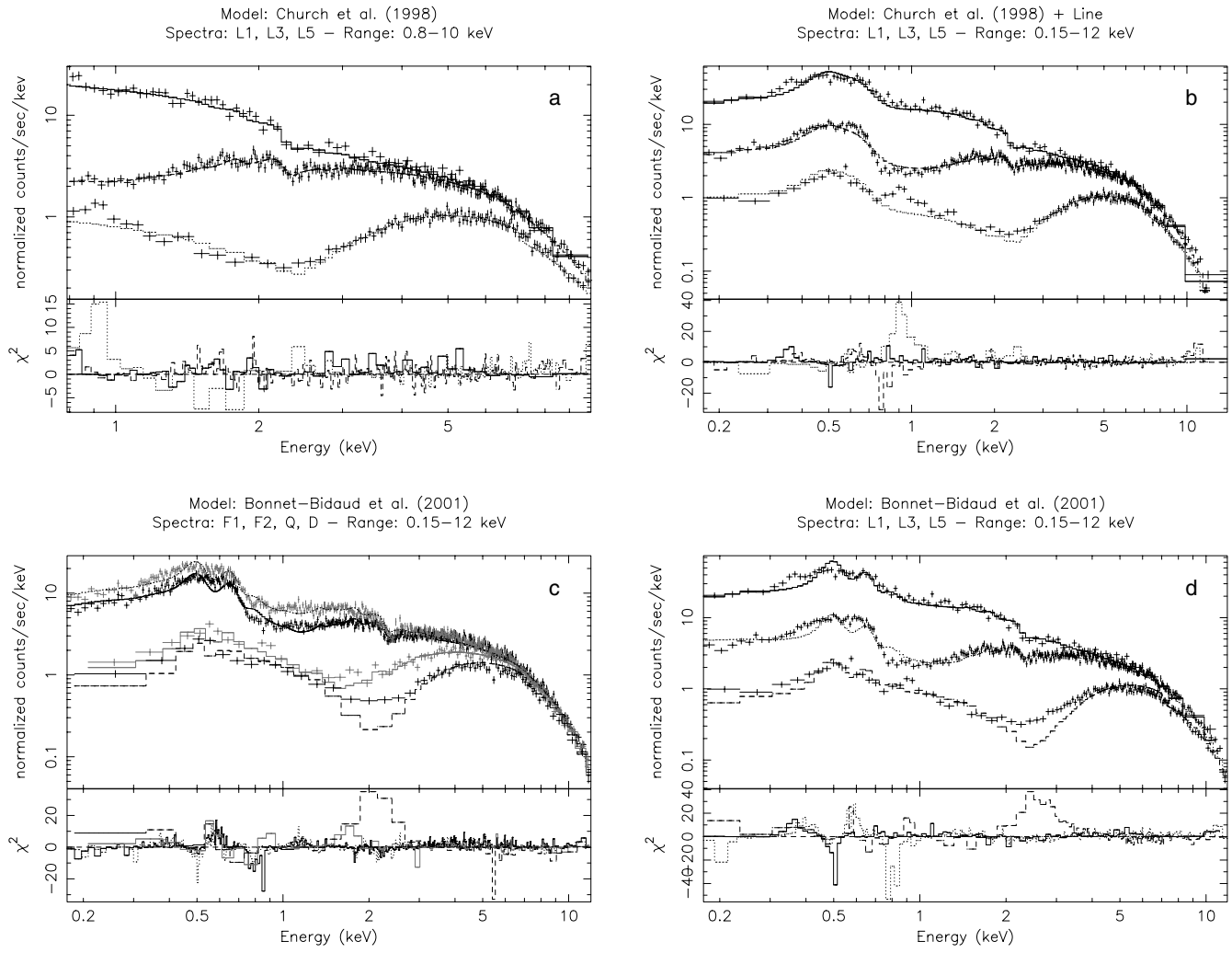

Fig. A.3. Model fits to various XMM–Newton spectra of EXO 0748–676. Spectra, models, and energy ranges are given above each panel. All spectra were rebinned for display purposes. In the panels **a)**, **b)**, and **d)** spectra L5, L3 and L1 are plotted from plot to bottom. In panel **c)** the order of the spectra, from top to bottom, is F2, F1, Q and D. See Table A.3 for fit parameters.

The first fits with the Bonnet-Bidaud et al. (2001) model were made to the time selected 0.15–12.0 keV spectra. The element abundances were fixed to the values found by Bonnet-Bidaud et al. (2001), while the other parameters were allowed to vary. The power law index, the power law normalization and the temperature of the thermal component were treated as single parameters in the joint fit to all four spectra. We obtain very similar values as Bonnet-Bidaud et al. (2001), but with a slightly higher $\chi^2_{\rm red}$ of 1.34 (d.o.f. = 2904) compared to their $\chi^2_{\rm red}$/d.o.f. = 1.27/2467. This difference can be partly attributed to a different grouping of the data (minimum of 25 counts per bin instead of 20), higher maximum energy (12 keV instead of 10 keV), and also due to improved calibration of the instruments. In any case, as is clear from Fig. A.3, large localized residuals and broad deviations are present; e.g. in the fit to the dip spectrum around 2 keV, and in the fits to the flare and quiescent spectra above 3 keV.

Bonnet-Bidaud et al. (2001) do not argue why they did not treat the normalization of the thermal component as a single parameter for all four spectra, as they did for the normalization of the power law component. It is not clear to us why the properties of an extended component would vary on a shorter time scale than those of a compact component. Their argument that the increases in the normalization of the thermal component are due to reprocessing of energy from type I X-ray bursts is not supported by our observations of bursts and flaring intervals. The increases in the normalization occur with decreases in the absorption of the thermal component, suggesting that the variable normalization tries to compensate for the absence of a progressive covering factor in the model. Indeed, tying the value of the normalization to a single parameter results in a $\chi^2_{\rm red}$ of 1.92.

Next we fitted the Bonnet-Bidaud et al. (2001) model (i.e. without tying the normalization of the thermal component, to stay consistent with the previous fit) to our intensity selected spectra L1, L3, and L5 with the abundances of N, O, Ne, and Mg left free to vary. Using the fit-results from the time selected spectra as a starting point we obtained a $\chi^2_{\rm red} \sim 1.6$ with similar fit parameters. However, a lower $\chi^2_{\rm red}$ of 1.53 was obtained with a higher temperature and a much higher abundance of N (~80 times solar compared to ~10 times); these fit results can be found in Table A.3 and are shown in Fig. A.3d. Again

Table A.3. Spectral fit results. Models and energy ranges are given for each of the fits. All errors represent 1σ confidence intervals.

	Model: Bonnet-Bidaud et al. (2001) Range: 0.15–12 keV $\chi^2_{\rm red}$/d.o.f. = 1.35/2904				Model: Bonnet-Bidaud et al. (2001) Range: 0.15–12 keV $\chi^2_{\rm red}$/d.o.f. = 1.54/1914		
	F1	F2	Q	D	L5	L3	L1
APL (^{a})	1.82(2)	1.28(2)	5.7(1)	11.6(2)	1.34(6)	2.77(3)	17.9(3)
$\Gamma_{\rm pl}$	1.29(1)				1.44(1)		
$N_{\rm pl}$ (^{b})	$2.19(1)\times10^{-2}$				$2.85(2)\times10^{-2}$		
ARS (^{a})	0.048(1)	0.052(1)	0.18(1)	0.24(1)	0.033(2)	0.010(1)	0.110(4)
$kT_{\rm RS}$ (keV)	0.50(1)				1.42(3)		
$N_{\rm RS}$ (^{c})	$3.35(4)\times10^{-2}$	$4.86(5)\times10^{-2}$	$2.0(1)\times10^{-2}$	$1.98(6)\times10^{-2}$	$3.79(1)\times10^{-2}$	$5.6(1)\times10^{-3}$	$2.77(5)\times10^{-3}$

^{a} 10^{22} atoms cm^{-2}; ^{b} photons keV^{-1} cm^{-2} s^{-1} at 1 keV; ^{c} $10^{-14}/(4\pi D_{\rm A}^2)\int n_{\rm e} n_{\rm H} {\rm d}V$, with where $D_{\rm A}$ is the angular size distance to the source (cm), $n_{\rm e}$ is the electron density (cm^{-3}), and $n_{\rm H}$ is the hydrogen density (cm^{-3}).

large residuals are present around 2–3 keV in the L1 spectrum. Unlike the fit to the time selected spectra, here the normalization and the absorption of the extended component do not correlate.

A.2.3. Eclipse spectrum

A powerful test of both spectral models can be made with the spectrum obtained during the eclipse. As the compact component is eclipsed, one expects to see mainly contribution from the extended component. In the Church et al. (1998) model this is the (progressively covered) power law + Gaussian combination and in the Bonnet-Bidaud et al. (2001) model this is the thermal halo. A fit with a power law + Gaussian at 0.52 keV gives $\chi^2_{\rm red}$/d.o.f. = 1.5/18, whereas the fit with the Raymond-Smith model gives $\chi^2_{\rm red}$/d.o.f. = 1.9/15. It should be noted that for the latter model we obtain both very high temperatures and abundances. Fixing these parameters to more reasonable values (like those obtained from the fits to the non-eclipse spectra) gives a $\chi^2_{\rm red}$ values of 3.5-5, with large positive residuals above 2 keV.

Given the strong indications that the scattered/reflected light from compact source/neutron star *does* contribute to the eclipse in this source – as suggested by observations of type I X-ray bursts during eclipse (Parmar et al. 1985; Gottwald et al. 1987) – it is not surprising that both models fail to fit the eclipse spectrum. We therefore include the compact components again in both models, keeping in mind that 1) their contribution should be around 5% of that measured outside eclipse (i.e. the percentage of scattered flux measured for the type I X-ray bursts in eclipse) and 2) that the $N_{\rm H}$ for this component should not be larger than that during dips, as the scattered light should be much less affected by the absorbing structures. Adding the black body (with kT fixed to 1.46) to the power law + Gaussian combination does not lead to a significant improvement of the fit. However, adding a power law (with index fixed to 1.35) to the Raymond-Smith model and fixing all abundances to 1 leads to a much improved fit: $\chi^2_{\rm red}$/d.o.f. = 1.12/19, with $kT_{\rm RS} \sim 0.4$ keV. The normalization of the power law component in this fit is ∼2−3% of that in the fits to the non-eclipse data and the $N_{\rm H}$ is $\sim 8 \times 10^{21}$ atoms cm^{-2}, in reasonable agreement with our expectations and also similar to the results obtained from eclipse spectra in MXB 1659–298 (Sidoli et al. 2001). Assuming that a considerable part of the reflecting/scattering medium is obscured during the eclipse, it is quite likely that the contribution to the spectrum of this reflected/scattered component is considerably higher outside of eclipse, partly explaining the problems encountered when fitting those spectra.

A.3. Concluding remarks

Our fits clearly show that current models are not able to fit the absorption affected spectra of EXO 0748–676 during dips. While the fits to the eclipse spectrum favor the thermal halo model of Bonnet-Bidaud et al. (2001) this model has severe problems with the deep dip spectra. Our eclipse spectrum provided strong evidence for the presence of an additional scatter/reflection component, which should be an integral part in future models. Such models should also include more advanced models for the absorbing material and also for the structure of the thermal halo.

References

Arnaud, K. A. 1996, in Astronomical Data Analysis Software and Systems V, ASP Conf. Ser., 101, 17

Bonnet-Bidaud, J. M., Haberl, F., Ferrando, P., Bennie, P. J., & Kendziorra, E. 2001, A&A, 365, L282

Church, M. J., Balucinska-Church, M., Dotani, T., & Asai, K. 1998, ApJ, 504, 516

Cottam, J., Kahn, S. M., Brinkman, A. C., den Herder, J. W., & Erd, C. 2001, A&A, 365, L277

Cottam, J., Paerels, F., & Mendez, M. 2002, Nature, 420, 51

Crampton, D., Stauffer, J., Hutchings, J. B., Cowley, A. P., & Ianna, P. 1986, ApJ, 306, 599

Dickey, J. M., & Lockman, F. J. 1990, ARA&A, 28, 215

Frank, J., King, A., & Raine, D. 1992, Accretion Power in Astrophysics, Accretion Power in Astrophysics, ISBN 0521408636 (Cambridge University Press)

Frank, J., King, A. R., & Lasota, J. 1987, A&A, 178, 137

Gottwald, M., Haberl, F., Parmar, A. N., & White, N. E. 1986, ApJ, 308, 213

Gottwald, M., Haberl, F., Parmar, A. N., & White, N. E. 1987, ApJ, 323, 575
Hertz, P., Wood, K. S., & Cominsky, L. R. 1997, ApJ, 486, 1000
Homan, J., Jonker, P. G., Wijnands, R., van der Klis, M., & van Paradijs, J. 1999, ApJ, 516, L91
Homan, J., & van der Klis, M. 2000, ApJ, 539, 847
Jansen, F., Lumb, D., Altieri, B., et al. 2001, A&A, 365, L1
Jimenez-Garate, M. A., Schulz, N. S., & Marshall, H. L. 2003, ApJ, 590, 432
Jonker, P. G., van der Klis, M., Homan, J., et al. 2000, ApJ, 531, 453
Jonker, P. G., van der Klis, M., & Wijnands, R. 1999, ApJ, 511, L41
Larwood, J. 1998, MNRAS, 299, L32
Liu, Q. Z., van Paradijs, J., & van den Heuvel, E. P. J. 2001, A&A, 368, 1021
Lubow, S. H., & Shu, F. H. 1976, ApJ, 207, L53
Melia, F., Zylstra, G. J., & Fryxell, B. 1991, ApJ, 377, L101
O'Donoghue, D., & Charles, P. A. 1996, MNRAS, 282, 191
Parmar, A. N., White, N. E., Giommi, P., & Gottwald, M. 1986, ApJ, 308, 199
Parmar, A. N., White, N. E., Giommi, P., & Haberl, F. 1985, IAU Circ., 4039
Retter, A., Chou, Y., Bedding, T. R., & Naylor, T. 2002, MNRAS, 330, L37
Sidoli, L., Oosterbroek, T., Parmar, A. N., Lumb, D., & Erd, C. 2001, A&A, 379, 540
Strüder, L., Briel, U., Dennerl, K., et al. 2001, A&A, 365, L18
Thomas, B., Corbet, R., Smale, A. P., Asai, K., & Dotani, T. 1997, ApJ, 480, L21
Turner, M. J. L., Abbey, A., Arnaud, M., et al. 2001, A&A, 365, L27
van der Klis, M. 2000, ARA&A, 38, 717
Walter, F. M., Mason, K. O., Clarke, J. T., et al. 1982, ApJ, 253, L67
Warner, B. 1995, Ap&SS, 226, 187
White, N. E., & Swank, J. H. 1982, ApJ, 253, L61